Stability of a semiconductor laser with a dispersive extended cavity

L. Ramunno and J. E. Sipe
Department of Physics, University of Toronto, 60 St. George Street, Toronto, Ontario, Canada M5S 1A7
(Received 30 April 2002; published 26 September 2002)

We present a theoretical investigation of the stability properties of semiconductor lasers with strong feedback from dispersive extended cavities. Surprisingly, unstable behavior had been observed experimentally for chirped fiber grating lasers, where the stability of the laser was found to depend upon the *orientation* of the fiber grating. We reproduce this finding through a linear stability analysis, demonstrating that the presence of both the linewidth enhancement of the semiconductor diode, and a negative curvature of the phase of the external cavity reflection coefficient are necessary for instability to occur. In order to explain the role of the linewidth enhancement and phase curvature, we present a second approach based on more approximate model wherein the field evolution is found to be described by an equation that resembles the nonlinear Schrödinger equation (NLSE); the curvature of the phase then corresponds to the dispersion coefficient of a usual NLSE, and the linewidth enhancement factor corresponds to the nonlinear coefficient. We find an unstable regime analogous to the anomalous dispersion regime of the usual NLSE, where the boundary between normal and anomalous dispersion depends upon the width of the reflectivity spectrum. We also find that there is an additional unstable region that arises due to the carrier dynamics, and has no analogy in systems with an instantaneous nonlinearity. Further, for lasers with a negatively chirped grating, we find that oscillation tends to occur on the red side of the reflection spectrum peak.

DOI: 10.1103/PhysRevA.66.033817 PACS number(s): 42.55.Px, 42.60.Mi

I. INTRODUCTION

Extended cavity semiconductor lasers with strong dispersive external feedback are of current interest for many different technological applications, including fiber grating semiconductor lasers for wavelength division multiplexing (WDM) applications [1–7], diffraction grating coupled semiconductor lasers for broad range tunability [8,9], as well as a variety of other applications that require stable cw operation [10,11]. Typically, these extended-cavity semiconductor lasers are composed of two elements: a semiconductor laser diode with an antireflection (AR) coated facet and, coupled to this facet, a strongly dispersive, passive, external reflector that forms an extended laser cavity. The dispersive reflector is chosen such that the width of its reflection spectrum is much narrower than the width of the gain spectrum of the semiconductor active medium, with the usual purpose of providing wavelength selectivity in order to ensure that the laser operates stably near a single longitudinal mode of the laser diode; this is often very effective. Quite unexpectedly, however, experiments showed that the stability of cw operation of lasers using chirped fiber gratings as external reflectors is drastically altered by simply changing the *orientation* of the fiber grating [6]. For lasers with a fiber grating placed such that the index modulation period decreased with distance from the AR coated diode facet (negative grating chirp), as drawn schematically in Fig. 1(a), stable single mode operation occurred. However, the opposite grating orientation (positive grating chirp), as in Fig. 1(b), produced significant laser instability, resulting in a complicated multimode behavior. This at first seems counter intuitive, since the reflectivity spectra of both gratings are identical. Only the sign of the phase curvature of the reflection coefficient is affected by the directionality of the grating chirp, and this has been shown to play only a small role in large-scale current modulation dynamics [12]. In this paper, we present a theoretical stability analysis of dispersive extended cavity semiconductor lasers [13] that examines, in particular, the role of the external reflector dispersion.

We begin in Sec. II with a presentation of the laser equations that are used in the analyses of this paper. We adopt a model for the semiconductor diode developed earlier [14], which is based on a standard coupled traveling-wave phenomenological approach; although the diode model we adopt is no more complicated to use than usual rate equation models [15,16], it is much more accurate [12]. It does not rely on the assumption that gain is uniform along the length of the diode, an assumption that is typically made but often inappropriate [12], but instead assumes that any relevant time scales of the problem of interest—such as, in the system we consider here, the extended laser cavity round trip time, or the time scale of the growth of any instabilities—are much longer than the round trip time of light in the diode itself.

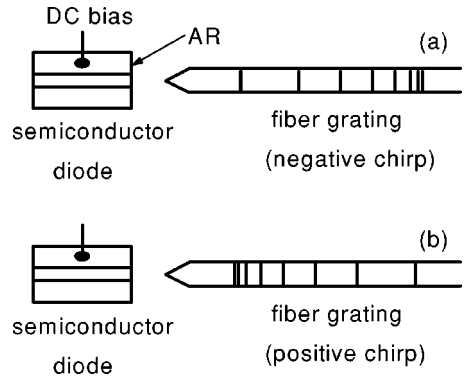

FIG. 1. Schematic drawings of antireflection (AR) coated semiconductor diodes coupled to chirped fiber gratings that form an extended laser cavity. In (a), the grating index of refraction modulation period decreases with distance from the AR facet (negative chirp); this laser was found in experiments to operate in a stable, single mode. The grating in (b) has the opposite orientation (positive chirp) and was found to be unstable in experiments.

Additionally, the form of the model is such that it is easily applicable to the study of systems consisting of multiple elements, such as extended-cavity lasers. The laser equations themselves are finally derived using an arbitrary complex reflection spectrum that describes the frequency domain response of the dispersive external reflector.

In Sec. III we perform a linear stability analysis of our full laser equations, keeping the analytical form of the reflection spectrum completely arbitrary. Assuming that the laser is initially in cw operation, and oscillating at some nominal lasing frequency within the bandwidth of the dispersive reflector, we seek the response of the electric field to small perturbations from steady state. We find an expression for the Laplace transform of the field response, and assess the stability of a particular cw mode of the laser simply by locating the singularities of the transform over the complex plane; we need not choose an explicit analytical form for the reflection function, since here we do not consider the laser response explicitly in the time domain. The singularities of the field transform that are obtained correspond directly to the Fabry-Perot resonances of the extended laser cavity, and any instability that would occur initiates from growth of the amplitude(s) of one (or more) of these cavity modes. We find that, for a negatively chirped fiber grating laser similar to the experimental configuration described above [6], there are no exponentially growing solutions for a cw mode at the peak of the reflection spectrum. For a positively chirped fiber grating laser, however, there are exponentially growing solutions, indicating instability.

Though we can explain many features of the laser stability and the behavior of the laser cavity resonances with the Laplace transform formalism of Sec. III, we also seek a more physical understanding of the role of the external reflector dispersion in stability determination. To this end, we present in Sec. IV a more approximate laser model that further assumes that the time scale of the growth of instabilities is much longer than the round trip time of light in the total laser cavity, and uses a Taylor expansion of the reflection coefficient in order to describe the dispersion with only a few parameters. We then find that the time evolution of the field is described by an equation resembling a nonlinear Schrödinger equation (NLSE). Through an extension of well-known work on other physical systems described by the usual NLSE [17], we can then describe the effects of the external cavity dispersion on laser dynamics. We find, for example, that the curvature of the phase of the reflection coefficient corresponds to the ''dispersion coefficient'' of the usual NLSE, and that the semiconductor diode linewidth enhancement factor corresponds to the ''nonlinear coefficient.'' The instabilities that occur in the cw solutions of our equations are seen to be analogous to the modulational instability of uniform solutions of the NLSE. Unlike the usual modulational instability, however, the frequencies at which unstable growth may occur in our system are limited to a discrete set. As we find with the Laplace transform formalism of Sec. III, these frequencies correspond to the Fabry-Perot resonances of the laser cavity—the modulational instability calculation then determines the growth or decay rates of these modes. As expected, we find that our modulational instability results agree well with the results of the Laplace transform formalism of Sec. III.

The calculation of the modulational instability, even if slightly less accurate, is quite straightforward numerically—in fact, far less cumbersome than using the Laplace transform formalism. For this reason, and to allow a direct comparison with the known analytical results of the modulational instability of the usual NLSE, we use our second formalism to examine more closely laser stability as a function of the curvature of the reflection spectrum phase. In contrast to usual modulational instability results, we find that the stability is only possible for a bounded range of the dispersion parameter. This bounded range is not symmetric about zero phase curvature, but is centered on the positive side. This suggests that lasers with reflectors with positive phase curvatures are more likely to fall within this stable range than lasers with negative curvature, as we would expect from experimental results described earlier. The lower bound is set by both the width of the reflectivity spectrum and the linewidth enhancement factor of the diode, and is analogous to the boundary between the anomalous and normal dispersion regimes given by the usual NLSE. The upper bound arises from the presence of carrier dynamics, and thus has no correspondence to systems that are adequately described by an instantaneous nonlinearity. Further, we find that for stable lasers with a reflection phase curvature corresponding to negatively chirped fiber gratings, the laser tends to operate on the red side of the reflection spectrum.

Our conclusions are presented in Sec. V.

II. LASER MODEL

In this section, we develop a model for the laser that combines a description of the time domain response of a diode developed earlier [12,14] with the frequency response of the dispersive reflector. Since the coupling diode facet is AR coated, and the effective feedback strengths typical for the dispersive reflectors we consider here allow the laser operation to occur in the strong feedback regime—often referred to as regime V in the literature on external cavity semiconductor lasers [18,19]—we can treat the extended laser as a single cavity. The diode description we use is based on a standard set of phenomenological, coupled partial differential equations [14,20] describing the dynamics of the electron-hole (carrier) density, $N(z,t)$, and the forward- and backward-propagating envelope functions, $E_+(z,t)$ and $E_-(z,t)$, defined by

$$E(z,t)=E_+(z,t)e^{ik_o z-i\omega_o t}+E_-(z,t)e^{-ik_o z-i\omega_o t}+\text{c.c.},$$

where $E(z,t)$ is the electric-field amplitude of the transverse mode of interest. We later set the reference frequency ω_o to be the operating frequency of the laser, and k_o the associated wave number. The main assumption of the diode description [14] is that the round trip time of light within the diode itself is much shorter than other time scales of interest. For the laser we examine in this paper, these other time scales include the laser round trip time and the characteristic times for growth of instabilities. Under this assumption, the diode dy-

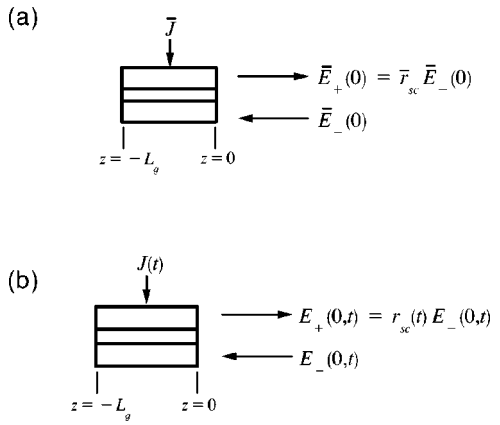

FIG. 2. Schematic illustration of (a) steady state and (b) dynamic operation of the semiconductor diode. The steady-state gain is characterized by $\bar{r}_{sc}$, and the dynamical gain by $r_{sc}(t)$.

namics are found to be very well described by a single ordinary differential equation for an average carrier density that depends on the field only at the diode AR facet, and a time-dependent reflection function that gives an explicit relationship between the output and input fields; the diode can thus be treated as a ''black box.'' Unlike typical rate equation models [15,16], uniformity in the carrier density and intensity along the diode is not assumed; yet the form of the equations in this diode description are no more complicated than rate equations.

The dynamical equation and reflection coefficient that appear in the diode description are referenced to a particular steady state of the diode characterized by three parameters: the bias current density $\bar{J}$, a steady-state diode reflection coefficient $\bar{r}_{sc}$, and an input field $\bar{E}_-(z=0)$, as illustrated in Fig. 2(a), where the output field is related to the input by $\bar{E}_+(0)=\bar{r}_{sc}\bar{E}_-(0)$; we choose $z=0$ to indicate the location of the coupling between the diode and external reflector at the AR coated diode facet. The diode steady-state quantities are all denoted by an overbar, and are found by solving the time-independent versions of the phenomenological equations [12,14]. Any steady state can be used for this reference, although in practice it is convenient to use the nominal operating point of the laser.

We define the average carrier density above steady state by

$$N_{av}(t)=\frac{1}{L_g}\int_{-L_g}^{0}[N(z,t)-\bar{N}(z)]dz,$$

where L_g is the diode length; $\bar{N}(z)$ is the steady-state carrier density profile that is the solution of the time-independent version of phenomenological equations for a given $\bar{J}$ and $\bar{r}_{sc}$. The time evolution of $N_{av}(t)$ is then given by [12,14]

$$\frac{dN_{av}}{dt}=\frac{J(t)-\bar{J}}{ed}-\frac{N_{av}}{T_n}+\frac{2}{T_g\Gamma}\bar{S}_+(0)\left[1+\frac{(1-R^2)}{R|\bar{r}_{sc}|}-\frac{1}{|\bar{r}_{sc}|^2}\right]-\frac{2}{T_g\Gamma}S_+(0,t)\left[1+\frac{(1-R^2)}{R|r_{sc}(t)|}-\frac{1}{|r_{sc}(t)|^2}\right], \quad (1)$$

TABLE I. Semiconductor diode parameters.

Parameter	Symbol	Typical value
Differential gain	a	2.22×10^{-16} cm^2
Linewidth enhancement factor	β_c	2
Carrier recombination time	T_n	1 ns
Mode confinement factor	Γ	0.34
Effective waveguide thickness	d	0.15 μm
Background index of refraction	n_g	3.7
Diode length	L_g	250 μm
Reflectivity of back diode facet	R^2	1
Group velocity in diode	$v_g\equiv c/n_g$	0.81×10^8 m/s
Round trip time in diode	$T_g\equiv 2L_g/v_g$	6.17 ps

where e is the electronic charge and $J(t)$ is the time-dependent current density; $r_{sc}(t)$ is the time-dependent reflection function governing the gain of the diode, as illustrated in Fig. 2(b), and is given explicitly by [12,14]

$$r_{sc}(t)\equiv\frac{E_+(0,t)}{E_-(0,t)}=\bar{r}_{sc}e^{(1-i\beta_c)L_g\Gamma a N_{av}(t)}. \quad (2)$$

The various diode parameters that appear in Eqs. (1) and (2) are identified in Table I, and have been discussed earlier [14] in the context of the phenomenological model; S_+ is an effective photon density corresponding to the forward-propagating field, where

$$\bar{S}_+(0)=\frac{n_g^2}{2\pi\hbar\omega_o}|\bar{E}_+(0)|^2,$$

$$S_+(0,t)=\frac{n_g^2}{2\pi\hbar\omega_o}|E_+(0,t)|^2,$$

where n_g is the index of refraction in the unpumped gain medium. To simplify the subsequent analysis we have excluded gain compression from the diode model, although it can be included, and indeed is in the original diode description [14]. Since we consider only laser operation at a fixed bias current, the gain changes due to gain compression are small during the evolution of the dynamics of the field and carrier density about their steady states. Gain compression is important, however, in the description of the large-scale current modulation discussed earlier [12].

Next we consider the frequency domain response of the dispersive reflector. Defining the Fourier components of the field envelope functions at the diode-reflector boundary by

$$E_\pm(0,t)=\int\frac{d\Omega}{2\pi}e^{-i\Omega t}\tilde{E}_\pm(0,\Omega), \quad (3)$$

where $\Omega\equiv\omega-\omega_o$ is the detuning for frequency ω, the reflection coefficient is then expressed as a ratio of the reflector,

$$\tilde{E}_-(0,\Omega)=\tilde{r}(\Omega)\tilde{E}_+(0,\Omega). \quad (4)$$

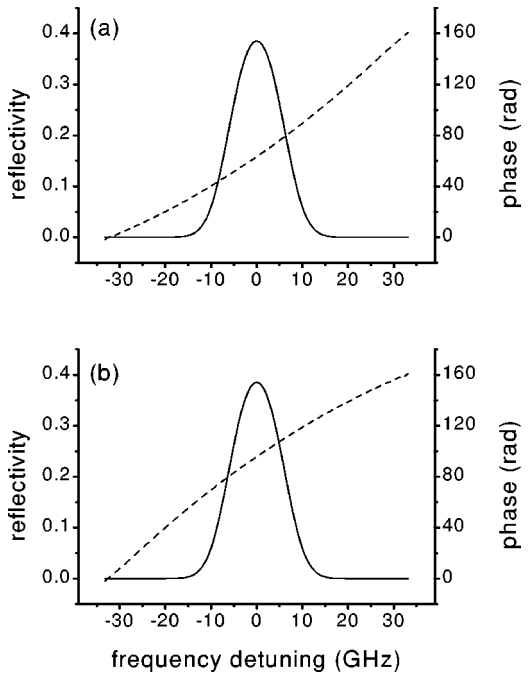

FIG. 3. Calculated reflection spectra (solid lines) and phases (dashed lines) corresponding to oppositely oriented fiber gratings that are similar to those used in the experiments of Morton *et al.* [6] The index profiles of both (a) and (b) are Gaussian with a full width at half maximum (FWHM) of 1 cm, a (maximum) index modulation depth of 3×10^{-5}, and a uniform background index of 1.44; the period of modulation at the center of the gratings corresponds to a vacuum wavelength of 1535 nm. The linear grating chirp for (a) is -1 Å/cm, and for (b) is 1 Å/cm.

For a given reflector, $\tilde{r}(\Omega)$ can be determined in principle through direct measurement; more usually it is calculated from a realistic model of the reflector. For fiber gratings, for example, $\tilde{r}(\Omega)$ is easily calculated by solving a pair of coupled-mode equations [21]. Figures 3(a) and 3(b) show the reflection coefficients and corresponding phases for negatively and positively chirped fiber gratings similar to those used in the experiments of Morton *et al.* [6,22]. Note that the reflectivity spectrum is the same for both orientations, but the corresponding phases have opposite curvature; we will see that it is the phase curvature that is important in the determination of the stability of single mode operation. In order to obtain a clearer qualitative understanding of the role of this curvature in stability in the following section, the width of the reflection spectrum for this set of calculations is somewhat smaller than that of the fiber gratings used in the experiments. In a later calculation, however, we do consider a grating spectral width that corresponds to the experimental width.

We obtain from Eqs. (3) and (4) the time domain response of the reflector, given by

$$E_-(0,t)=\int_{-\infty}^{\infty}\frac{d\Omega}{2\pi}e^{-i\Omega t}\tilde{r}(\Omega)\tilde{E}_+(0,\Omega) \tag{5}$$

$$=\int_{-\infty}^{t}dt'r(t-t')E_+(0,t'). \tag{6}$$

The response function

$$r(t)\equiv\int\frac{d\Omega}{2\pi}r(\Omega)e^{-i\Omega t}$$

is such that $r(t)=0$ for $t<0$, and for $\tilde{r}(\Omega)$ defined over the complex Ω plane, all the singularities must occur only in the lower half plane.

We now combine the responses of the diode and external reflector to obtain the laser equations. First we find the discrete cw cavity modes of the laser, Ω_m, given by solutions to

$$1=\bar{r}_{sc}(\Omega)\tilde{r}(\Omega), \tag{7}$$

where the frequency dependence of $\bar{r}_{sc}$ is given explicitly in earlier work [12,14]. Denoting the nominal lasing frequency by subscript "0," we have by definition $\Omega_0=0$. The value of $\bar{r}_{sc}$ is thus set by the value of the reflection function at the lasing mode, $\tilde{r}_o\equiv\tilde{r}(0)$. In steady state, $N_{av}=0$ and the fields at the $z=0$ diode facet are given by $\bar{E}_{\pm}(0)$. To simplify the subsequent analysis, we write the final form of the dynamical equations in terms of normalized carrier density and field functions, defined by

$$\sigma(t)=2L_g\Gamma aN_{av}(t),$$

$$\xi(t)=E_+(0,t)/\bar{E}_+(0),$$

and in terms of a normalized field intensity

$$\bar{s}_+=v_g aT_n\bar{S}_+(0);$$

then $\xi=1$ and $\sigma=0$ in steady-state operation. The dynamical equations then become

$$T_n\frac{d\sigma}{dt}=-\sigma(t)+2\bar{s}_+\left[1+\frac{(1-R^2)}{R|\bar{r}_{sc}|}-\frac{1}{|\bar{r}_{sc}|^2}\right]$$
$$-2\bar{s}_+|\xi(t)|^2\left[1+\frac{(1-R^2)}{R|r_{sc}(t)|}-\frac{1}{|r_{sc}(t)|^2}\right], \tag{8}$$

obtained from Eq. (1), and

$$\xi(t)=r_{sc}(t)\int_{-\infty}^{\infty}\frac{d\Omega}{2\pi}e^{-i\Omega t}\tilde{r}(\Omega)\tilde{\xi}(\Omega)$$

$$=r_{sc}(t)\int_{-\infty}^{t}dt'r(t-t')\xi(t'), \tag{9}$$

obtained from Eqs. (2), (5), and (6), where the reflection coefficient in terms of $\sigma(t)$ is

$$r_{sc}(t)=\bar{r}_{sc}\exp\left(\frac{1}{2}(1-i\beta_c)\sigma(t)\right). \tag{10}$$

Note that Eq. (9) is the time-dependent version of Eq. (7), where the dynamics of the field $\xi(t)$ depends on all its previous values. Equations (8)–(10) form the starting point for our stability analyses that follow.

III. LINEAR STABILITY ANALYSIS

As a first step in our examination of laser stability, we perform a direct linear stability analysis of Eqs. (8) and (9) in order to characterize the response of the system to perturbations in the steady-state field and carrier density. In particular, we seek to find under what conditions the laser—initially oscillating at some nominal frequency within the bandwidth of the dispersive reflector—either returns to the cw operating mode as these perturbations decay away, or experiences a growth in the perturbations, leading to unstable behavior such as mode hopping. Due to the relatively long external cavity used in the experiments of Morton *et al.* [6], there are many available external cavity resonances within the width of the reflection spectrum that could be subject to unstable growth.

We define the (normalized) field deviation from steady state by

$$\psi = \xi - 1.$$

Then from Eqs. (7), (9), (10) we obtain

$$\psi(t) = (e^{(1/2)(1-i\beta_c)\sigma(t)} - 1) + \frac{e^{(1/2)(1-i\beta_c)\sigma(t)}}{\tilde{r}_o}\int_{-\infty}^{t} dt' r(t-t')\psi(t'), \quad (11)$$

where, recall, the value of the reflection function at the operating mode is $\tilde{r}_o$. Keeping only the terms linear in ψ and σ, the field equation (11) and the carrier density equation (8) become

$$\psi(t) = \frac{1}{2}(1-i\beta_c)\sigma(t) + \frac{1}{\tilde{r}_o}\int_{-\infty}^{t} dt' r(t-t')\psi(t'), \quad (12)$$

and

$$\frac{d\sigma(t)}{dt} = -\Gamma_1\sigma(t) - \Gamma_2[|1+\psi(t)|^2 - 1] \quad (13)$$

$$\simeq -\Gamma_1\sigma(t) - \Gamma_2[\psi(t) + \psi^*(t)], \quad (14)$$

respectively, where we have defined effective decay rates,

$$\Gamma_1 = \frac{1}{T_n}\left[1 + 2\overline{s_+}\left(|\tilde{r}_o|^2 - \frac{1}{2}\frac{(1-R^2)}{R}|\tilde{r}_o|\right)\right],$$

$$\Gamma_2 = \frac{1}{T_n}\left[2\overline{s_+}\left(1 + \frac{(1-R^2)}{R}|\tilde{r}_o| - |\tilde{r}_o|^2\right)\right]. \quad (15)$$

The carrier decay rate Γ_1 arises from both carrier relaxation (the "1" in the square brackets) and radiative recombination (the second term in the square brackets). The carrier-field coupling coefficient Γ_2 can also be seen as an effective decay rate for the field itself in the following way. Taking the derivative of Eq. (12), and then substituting Eq. (13) for $d\sigma/dt$, we see that the resulting equation for $d\psi/dt$ includes the term $-\Gamma_2[|1+\psi(t)|^2-1]/2$. For a field that deviates from cw, $\psi \neq 0$, and this term causes ψ to relax back to steady state. One can also show that $1/\Gamma_2$ is proportional to an effective photon lifetime often used to describe cavity losses in rate equation diode models, where the losses, occurring both at the back facet of the diode (R^2) and at the reflector ($|\tilde{r}_o|^2$), are assumed to be distributed evenly along the diode length.

We now seek the response of ψ to a perturbation of steady state occurring at $t=0$, given by

$$\sigma(0) = \varepsilon,$$

where ε is a small, real number. Taking the Laplace transforms of Eqs. (12) and (14), and subsequently solving for the Laplace transform $\hat{\psi}(s)$ of the field deviation function $\psi(t)$, we find

$$\hat{\psi}(s) = \frac{\frac{1}{2}\varepsilon(1-i\beta_c)\left[1 - \frac{\tilde{r}^*(is^*)}{\tilde{r}_o^*}\right]}{(s+\Gamma_1)\left[1 - \frac{\tilde{r}(is)}{\tilde{r}_o}\right]\left[1 - \frac{\tilde{r}^*(is^*)}{\tilde{r}_o^*}\right] + \frac{1}{2}\Gamma_2(1+i\beta_c)\left[1 - \frac{\tilde{r}(is)}{\tilde{r}_o}\right] + \frac{1}{2}\Gamma_2(1-i\beta_c)\left[1 - \frac{\tilde{r}^*(is^*)}{\tilde{r}_o^*}\right]}. \quad (16)$$

Both $\hat{\psi}(s)$ and the reflection functions

$$\tilde{r}(is) \equiv \int_0^\infty r(t)e^{-st}dt,$$

$$\tilde{r}^*(is^*) \equiv \left[\int_0^\infty r(t)e^{-s^*t}dt\right]^*,$$

are defined over the complex s plane. The values of $\tilde{r}$ on the

(negative) Ims axis correspond to those already defined in Eq. (4) with $\Omega = is$.

The linear stability of the laser can now be determined for a particular cw solution simply by finding the location of the singularities of $\hat{\psi}(s)$: any of these poles s_p located such that $\mathrm{Re}(s_p) > 0$ indicates exponentially growing solutions that oscillate with a frequency corresponding to $\mathrm{Im}(s_p)$. The poles' locations can be found by plotting contours of $\hat{\psi}(s)$ over the complex s plane, and this is easily accomplished given the appropriate reflection spectrum. For example, the calculation of $\tilde{r}$ over the complex plane for fiber gratings is straightforward, and is easily accomplished by allowing the frequency variable appearing in the coupled-mode equations to become complex. If $\tilde{r}$ is instead determined from measurement, and is thus known for real frequencies (and imaginary s), then to use Eq. (16) it would be necessary to extend this data by, for example, using a Taylor expansion of $\tilde{r}(\Omega)$ in order to make the frequency dependence explicit.

To gain some understanding of Eq. (16), we first consider the special case where the external reflector is a nondispersive mirror located some distance from the diode AR coated facet. We only use this as a toy model here; to describe such a physical system properly, we would of course have to take into consideration the shape of the gain curve of the diode. For the reflection coefficient of the form

$$\tilde{r}(\Omega) = A e^{i\Omega T_{ext}},$$

where T_{ext} is the round trip time in the external cavity and $|A|^2$ is the mirror reflectivity, the time domain response is a delta function $r(t) = A\,\delta(t - T_{ext})$, and from Eq. (16) we obtain

$$\hat{\psi}(s) = \frac{1}{2}\,\frac{\varepsilon(1 - i\beta_c)}{(s + \Gamma_1)(1 - e^{-sT_{ext}}) + \Gamma_2}. \tag{17}$$

Note that the semiconductor linewidth enhancement factor, β_c, is irrelevant in determining the locations of the singularities here.

We examine first the case where there is no carrier-field coupling by setting $\Gamma_2 = 0$. The poles of $\hat{\psi}(s)$ are then located at $s = -\Gamma_1$, and $s = i(2\pi m/T_{ext})$ for any integer m, as indicated in Fig. 4 by open circles, for a laser with diode parameters listed in Table I. The pole at $-\Gamma_1$ (not shown in Fig. 4) gives an exponentially decaying term. The other poles are located on the imaginary s-axis, and are equally distributed with a frequency spacing $2\pi/T_{ext}$; these correspond to the Fabry-Perot resonances of the laser cavity. Since they have a real part of zero, they neither decay nor grow. For a perturbation at $t = 0$, the Fabry-Perot cavity modes are initially excited, and they remain excited indefinitely as the field continues to oscillate at these frequencies with amplitudes determined by the initial perturbation. Even the amplitude of the nominal lasing mode at $\mathrm{Im}s = 0$ is itself not fixed, as the real part of the pole location is also zero. This is not surprising; in neglecting the carrier-field coupling we have also neglected field decay.

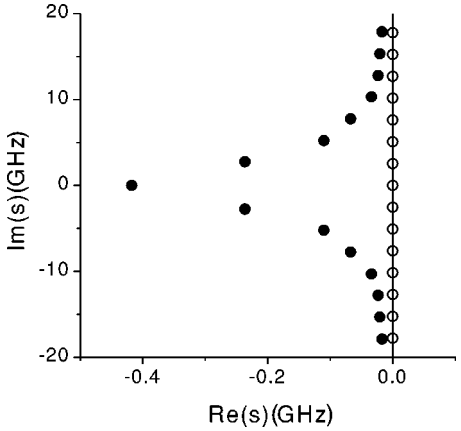

FIG. 4. Singularities of the Laplace transform of the field deviation from steady state, $\hat{\psi}(s)$, calculated over the complex s plane for a semiconductor diode coupled to an external nondispersive mirror. The diode is characterized by the parameters listed in Table I. The pole at $s = -\Gamma_1$ is not shown. The open circles indicate the pole locations for zero carrier-field coupling, and the filled circles indicate the pole locations for the case where carrier-field coupling is included. The external cavity roundtrip time is 388 ps.

If we now reinstate the carrier-field coupling coefficient Γ_2, the poles must be found numerically. We plot these also in Fig. 4 (filled circles), again for the diode parameters of Table I. The poles are now located away from the imaginary s axis in the left-hand s plane, indicating that the amplitudes of the oscillating resonances excited by the perturbation at $t = 0$ do experience decay, and the laser then returns to the original cw mode. The pole formerly at $s = 0$, corresponding to the nominal operating frequency, has shifted leftward the most of all the resonances, indicating that the decay rate is the largest for perturbations in the amplitude of the operating mode. Moving to the frequencies further and further from the operating frequency, the singularities move closer and closer to the imaginary s axis and thus experience smaller and smaller decay rates. To understand this, let us consider the effect on the rate of change of the carrier density caused by a field with amplitude $\overline{\psi}$ oscillating at a frequency $\overline{\Omega}$. From Eq. (14), we have

$$\frac{d\sigma(t)}{dt} = -\Gamma_1\sigma(t) - 2\Gamma_2|\overline{\psi}|\cos(\overline{\Omega}t + \delta), \tag{18}$$

where $\delta = -\arg\overline{\psi}$. If $\overline{\Omega}$ is far from $\Omega = 0$, then the second term on the right-hand side is rapidly oscillating, and its overall effect is negligible; the response is then indistinguishable from the $\Gamma_2 = 0$ limit, where the poles are located on the imaginary axis.

We mention the qualitative features of two more special cases that will be useful in interpreting the physics of the actual problem of interest. We first consider an external cavity where the reflection function is such that the spectrum along the imaginary s axis is as those plotted in Figs. 3(a) and 3(b), but the reflection coefficient phase has zero curvature. We examine, in particular, the stability of a cw solution that coincides with the reflection spectrum peak. As shown in

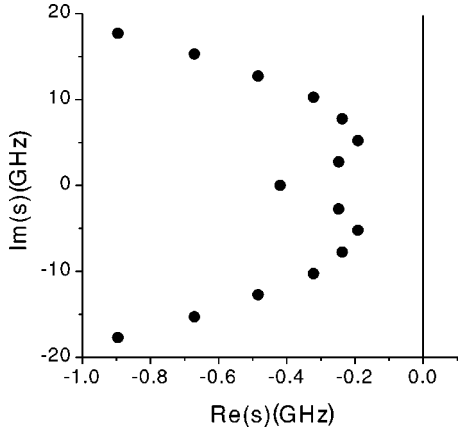

FIG. 5. Singularities of $\hat{\psi}(s)$ calculated for an external cavity laser with a reflectivity spectrum as shown by the solid lines of Figs. 3(a) and 3(b), but with zero reflection phase curvature. The diode parameters used are listed in Table I.

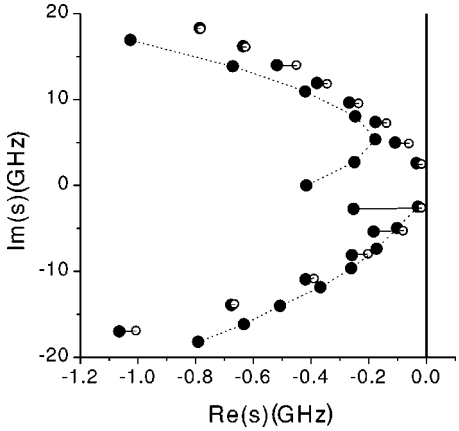

FIG. 6. Singularities (filled circles) and zeros (open circles) of $\hat{\psi}(s)$ calculated for an external cavity laser with a reflectivity spectrum and corresponding phase as shown in Fig. 3(a), but with the linewidth enhancement parameter set to zero. The zero-pole pairs corresponding to the ''shadow'' resonances are each shown as connected. The unpaired poles (true Fabry-Perot resonances) are connected to each other with a dotted line. The diode parameters used in this calculation are listed in Table I.

Fig. 5, and like the previous example, all singularities are located in the negative Res plane, indicating that perturbations decay and the field returns to its steady-state value. The resonance at Im$s=0$ has again a large decay rate, becoming progressively smaller for frequencies farther and farther from Im$s=0$. Beyond a certain Ims value, however, the singularities are located progressively farther from the imaginary s axis and the decay rates become progressively *larger*. This is a signature of the *shape* of a reflectivity spectrum with finite bandwidth, and results because at frequencies farther and farther from the reflection spectrum peak, the loss due to out coupling is greater and greater. Thus the amplitudes of modes excited far from Im$s=0$ experience faster decay for a reflection spectrum with finite width, than they would for a reflection spectrum that is completely flat. We will see that this feature survives for the realistic system we consider below.

But first we mention the results of a final special case, where we consider a laser with dispersive loss such as those shown in Figs. 3(a) and 3(b); we now include the effects of a nonzero phase curvature, but set the semiconductor linewidth enhancement factor β_c to zero. Here we find there are *two* sets of singularities that correspond to the Fabry-Perot cavity resonances, and one set of zeros, as shown in Fig. 6 for positive phase curvature. The zero locations (open circles) are given by the solutions to $\tilde{r}^*(is^*)=\tilde{r}_o^*$, and one set of the poles are located at nearly the same Im(s) location as the zeros, indicated in Fig. 6 by filled circles connected to these zeros. These zero-pole pairs are distributed along Im$s=-\mathrm{Re}(\Omega)$ such that the frequency spacing between the pairs is chirped. In this case of postive phase curvature, the spacing is larger for frequencies on the blue side of the reflection spectrum (Im$s<0$) than for those on the red side (Im$s>0$). The set of poles not associated with zeros (filled circles connected to each other with a dotted line) are also nonuniformly distributed along Ims, but chirped in the opposite direction of the zero-pole pairs. These unpaired poles are identified with the usual Fabry-Perot cavity resonances. Considering instead a reflector with negative phase curvature, we find that the chirps along Ims of the zero-pole pairs and the Fabry-Perot resonances are opposite to those shown for positive curvature in Fig. 6. In general, a nonzero phase curvature indicates dispersion in the external cavity round trip time for cw light. For fiber gratings, the phase curvature arises mainly from the chirp of the local period of the refractive index modulation. Since this period varies with length, the Bragg scattering condition is different at different locations along the grating. For a grating with a chirp such that the period decreases monotonically with distance (negative chirp), as illustrated in Fig. 7(a), incident light at longer wavelengths has a shorter round trip than light at shorter wavelengths. Since the derivative of the frequency dependent round trip time gives the curvature of the phase, a negative fiber grating chirp then corresponds to positive phase curvature. Additionally, since the effective external cavity

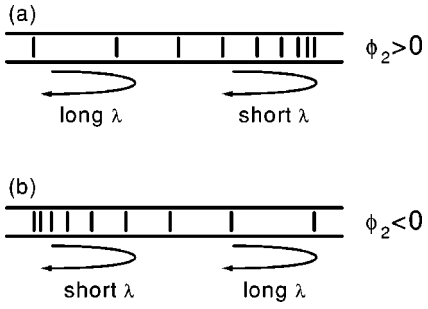

FIG. 7. Schematic illustrations of linearly chirped fiber gratings. Grating (a) is negatively chirped; longer wavelengths match the Bragg scattering at a location closer to the starting point than shorter wavelengths, and thus have a shorter laser round trip time. The corresponding reflection phase curvature is positive, so that $\phi_2>0$. Grating (b) is positively chirped; shorter wavelengths then have a smaller round trip time, and the phase curvature is negative, and $\phi_2<0$.

length is larger for blue frequencies and smaller for red frequencies, blue Fabry-Perot modes are more closely spaced than the red; this is what we find in Fig. 6. Conversely, a grating period that increases with distance (positive chirp), as illustrated in Fig. 7(b), corresponds to negative phase curvature, and red Fabry-Perot modes are more closely spaced than blue.

To understand the physical origin of the non-Fabry-Perot poles—i.e., those associated with the zeros and distributed along Ims with nonuniform mode distribution opposite to that of the Fabry-Perot resonances—we consider the initial and secondary laser responses to perturbation. We suppose that initially the system responds through the excitation of the ''true'' Fabry-Perot modes. Consider first only one of these excited resonances, say at frequency $\bar{\Omega}$, so that the field envelope deviation function is modified from its steady-state value of zero and is of the form $\psi=\bar{\psi}e^{-i\bar{\Omega}t}$; the total (real) forward-propagating electric field, and its intensity, is modulated from cw with a sinusoidal envelope function. Through stimulated emission, the field intensity acts as a source for the diode carrier density, evident from Eq. (18). The carrier density response to such a field is

$$\sigma(t)=-|\bar{\psi}|\frac{2\Gamma_2\Gamma_1}{\Gamma_1^2+\bar{\Omega}^2}\left(\cos(\bar{\Omega}t+\delta)+\frac{\bar{\Omega}}{\Gamma_1}\sin(\bar{\Omega}t+\delta)\right)$$

$$=-|\bar{\psi}|\frac{\Gamma_2\Gamma_1}{\Gamma_1^2+\bar{\Omega}^2}([1-i\bar{\Omega}/\Gamma_1]e^{i\delta}e^{i\bar{\Omega}t}$$

$$+[1+i\bar{\Omega}/\Gamma_1]e^{-i\delta}e^{-i\bar{\Omega}t}). \tag{19}$$

In turn, σ acts as a source for the field ψ, as evident in Eq. (12), causing the envelope function ψ itself to oscillate with sinusoidal dependence. It is clear from Eq. (12) and the second line of Eq. (19) that the effect of the carrier density oscillation is to create new frequency components of the electric field at $-\bar{\Omega}$; it is these secondary excitations resulting from carrier-field coupling that are the origin of the zero-pole pairs, or ''shadow'' Fabry-Perot modes. Indeed, neglecting this coupling by setting $\Gamma_2=0$ results in a single set of poles, as can be seen from Eq. (16). Note that for zero reflection phase curvature (and a symmetric spectrum), we do not see the extra zero-pole pair since the shadow mode frequencies are themselves Fabry-Perot modes. We see this mathematically by putting $\tilde{r}^*(is^*)=\tilde{r}(is)$ in Eq. (16). In both of these limits, the shadow poles of $\hat{\psi}$ are located in precisely the same location as the zeros of $\hat{\psi}$, and they effectively cancel each other.

We now turn finally to the stability of the more general case, by reinstituting the semiconductor linewidth enhancement factor β_c. In the previous special case with $\beta_c=0$, both sets of poles were located in the left-hand s plane indicating laser stability, and this was regardless of the sign of the phase curvature. Figure 8 shows the poles of $\hat{\psi}(s)$ calculated for the two lasers consisting of a diode as characterized in Table I, coupled to chirped fiber gratings with reflection spectra and phases as plotted in Figs. 3(a) and 3(b). Again, as a first measure of laser stability, we consider here the singularities in $\hat{\psi}(s)$ for a cw solution coinciding with the peak of the reflection spectrum. The open circles in Fig. 8 represent the location of the poles for the laser with the negative grating chirp; the singularities of $\hat{\psi}(s)$ are all found in the left-hand s plane indicating no growing solutions, suggesting that this laser configuration is stable. The filled circles in Fig. 8 give the location of the poles of $\hat{\psi}(s)$ for a laser with a grating of opposite orientation. Here we see that there are some modes that do indicate exponentially growing solutions, suggesting that this laser is unstable. The linewidth enhancement factor β_c thus plays a key role in the growth of instabilities since, at least in this linear analysis, instability does not occur when we set $\beta_c=0$.

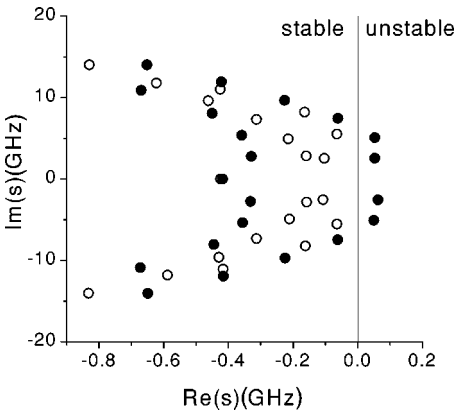

FIG. 8. Singularities of $\hat{\psi}(s)$ calculated for two lasers consisting of a diode described by parameters in Table I coupled to the chirped fiber gratings characterized in Figs. 3(a) and 3(b). The open circles indicate pole locations for the laser with the negatively chirped grating. All poles are located in the left-hand plane, indicating (linear) stability. The filled circles give the pole locations for an identical laser, but with a grating with opposite orientation. The poles such that $\mathrm{Re}(s)>0$ are susceptible to growth, indicating instability.

Although our analysis demonstrates the roles of the curvature of the reflection coefficient phase and the semiconductor linewidth enhancement in determining stability, it does not explain them. To study the stability analysis in more detail, we could, for example, choose an analytic form for $\tilde{r}(\Omega)$ that includes the phase curvature as one of the parameters—as we indeed do in the following section in another approach—but we found that this does not provide much insight into the problem. We now turn to an approximate description of the laser based on Eqs. (8)–(10) that does give such insight.

IV. MODIFIED NONLINEAR SCHRÖDINGER EQUATION

A. Formalism

In this section we present a derivation and discussion of approximate laser equations, obtained from our full laser model (8)–(10), where the field evolution is described by an equation that resembles a nonlinear Schrödinger equation. This allows us to describe and explain the effect on stability of the phase curvature of the reflection coefficient, and other

relevant parameters, in the context of the modulational instability of uniform solutions. To represent the reflection phase curvature of the extended cavity by one parameter, we approximate the reflection function by a Taylor expansion [12,15]

$$\tilde{r}(\Omega)=\tilde{r}_o\exp\left[(-\gamma_1+i\phi_1)\Omega+\frac{1}{2}(-\gamma_2+i\phi_2)\Omega^2+\cdots\right],$$

where the dispersion parameters γ_n, ϕ_n are defined by

$$\gamma_n=-\left.\frac{d^n\ln|\tilde{r}(\Omega)|}{d\Omega^n}\right|_{\Omega=0},$$

$$\phi_n=\left.\frac{d^n\arg[\tilde{r}(\Omega)]}{d\Omega^n}\right|_{\Omega=0}. \tag{20}$$

The external cavity round trip time (or delay) experienced by a long pulse centered at the operating frequency $\Omega=0$ is given by ϕ_1. The parameter ϕ_2, characterizes the round trip time dispersion. For fiber gratings, $\phi_2>0$ corresponds to negative grating chirp, and $\phi_2<0$ to a positive grating chirp, as noted in Fig. 7. The dispersion due to the shape of the reflectivity spectrum is described by the parameters γ_1 and γ_2—the slope and curvature of the negative logarithm of $|\tilde{r}(\Omega)|$, respectively—where the width of the reflection spectrum is proportional to $(\gamma_2)^{-1/2}$. For a laser operating frequency coinciding with the reflectivity peak, γ_1 is zero. In general, a lasing mode is on one side or the other of the reflectivity spectrum peak, the red side indicated by a negative value of γ_1, and the blue side by a positive γ_1. For lasers with long external cavities, as in the experiments of Morton *et al.* [6], the cw mode spacing is sufficiently small that there is always a mode reasonably close to the peak, so γ_1 is very small compared to ϕ_1. We find it useful for later analysis to define the complex dispersion quantity

$$\eta\equiv\frac{1}{2}\frac{\gamma_2-i\phi_2}{\phi_1^2},$$

and we note that for typical systems, especially those with long external cavities, $|\eta|\ll 1$. Rescaling the time variable in terms of the delay time ϕ_1,

$$\hat{t}\equiv\frac{t}{\phi_1},$$

the laser equations (9, 10) become

$$\xi(\hat{t})=e^{(1/2)(1-i\beta_c)\sigma(\hat{t})}\left[1-i\hat{\gamma}_1\frac{d}{d\hat{t}}+\eta\frac{d^2}{d\hat{t}^2}\right]\xi(\hat{t}-1), \tag{21}$$

where $\hat{\gamma}_1\equiv\gamma_1/\phi_1$, and where we keep only the first order in the expansion of the exponential function, since both $\hat{\gamma}_1$ and $|\eta|$ are much smaller than one.

In the limit of no dispersion and no carrier dynamics, Eq. (21) would be satisfied by any periodic function of $\hat{t}$ with a period of one. We then expect the solution for ξ to be an almost periodic function, with variations from periodicity due to dispersive effects and carrier dynamics. To capture this, we seek a multiple scales analysis solution of ξ of the form [23]

$$\xi(\hat{t})=\xi(\hat{t}_0,\hat{t}_1,\ldots), \tag{22}$$

where we define new independent time variables

$$\hat{t}_m=|\eta|^m\hat{t},$$

for $m=0,1,2,\ldots$, where recall $|\eta|\ll 1$; then

$$\frac{d}{d\hat{t}}=\frac{\partial}{\partial\hat{t}_0}+|\eta|\frac{\partial}{\partial\hat{t}_1}+\cdots. \tag{23}$$

The function ξ is assumed to vary significantly at most as each of its arguments $\hat{t}_m$ vary over unity. As the fastest time scale $\hat{t}_0$ varies from 0 to 1, real time varies from 0 to ϕ_1 and ξ advances by one laser round trip time. As $\hat{t}_1$ varies from 0 to 1, t varies from 0 to $\phi_1/|\eta|$, or many round trip times; it is on this slower time scale that we expect the growth of instabilities to occur. We insert Eqs. (22) and (23) into Eq. (21), and collect the terms that are multiplied by different powers of $|\eta|$; by requiring that the resulting equations be satisfied to higher and higher order in $|\eta|$, we expect an asymptotically better description of the dynamics. We further require that ξ be periodic in $\hat{t}_0$ with period unity

$$\xi(\hat{t}_0-1,\hat{t}_1-|\eta|,\ldots)=\xi(\hat{t}_0,\hat{t}_1-|\eta|,\ldots), \tag{24}$$

and since $|\eta|\ll 1$, we make the expansion

$$\xi(\hat{t}_0,\hat{t}_1-|\eta|,\ldots)\simeq\xi(\hat{t}_0,\hat{t}_1,\ldots)-|\eta|\frac{\partial\xi(\hat{t}_0,\hat{t}_1,\ldots)}{\partial\hat{t}_1}. \tag{25}$$

Substituting, Eqs. (23), (22), (24), and (25) into the field equation (21), and collecting the terms of zeroth and first order in $|\eta|$, we obtain

$$|\eta|\frac{\partial\xi(\hat{t}_0,\hat{t}_1)}{\partial\hat{t}_1}=(1-e^{-(1/2)(1-i\beta_c)\sigma(\hat{t}_0,\hat{t}_1)})\xi(\hat{t}_0,\hat{t}_1)$$
$$-i\hat{\gamma}_1\frac{\partial}{\partial\hat{t}_0}\xi(\hat{t}_0,\hat{t}_1)+\eta\frac{\partial^2}{(\partial\hat{t}_0)^2}\xi(\hat{t}_0,\hat{t}_1),$$

where we have neglected terms of order $|\eta|\hat{\gamma}_1$, and we consider only the two time scales $\hat{t}_0$ and $\hat{t}_1$. Now defining

$$x=\hat{t}_0,$$

$$\tau=\hat{t}_1/|\eta|,$$

we obtain for the field equation

$$i\frac{\partial\xi(x,\tau)}{\partial\tau}=\frac{1}{2}(\hat{\phi}_2+i\hat{\gamma}_2)\frac{\partial^2}{\partial x^2}\xi(x,\tau)+\hat{\gamma}_1\frac{\partial}{\partial x}\xi(x,\tau)$$
$$+i(1-e^{-(1/2)(1-i\beta_c)\sigma(x,\tau)})\xi(x,\tau), \qquad (26)$$

and for the carrier density equation (8)

$$\hat{T}_n\frac{\partial\sigma(x,\tau)}{\partial x}$$
$$=-\sigma(x,\tau)+2\overline{s}_+\left[1+\frac{(1-R^2)}{R|\overline{r}_{sc}|}-\frac{1}{|\overline{r}_{sc}|^2}\right]$$
$$-2\overline{s}_+|\xi(x,\tau)|^2\left[1+\frac{(1-R^2)}{R|\overline{r}_{sc}|}e^{-(1/2)\sigma(x,\tau)}-\frac{e^{-\sigma(x,\tau)}}{|\overline{r}_{sc}|^2}\right], \qquad (27)$$

where $\hat{T}_n=T_n/\phi_1$, $\hat{\gamma}_2=\gamma_2/\phi_1^2$, and $\hat{\phi}_2=\phi_2/\phi_1^2$. Note that the form of Eq. (26) is very similar to that of a usual nonlinear Schrödinger equation (NLSE). A standard method of assessing stability of systems described by a NLSE is through a modulational instability analysis, whereby the growth rates of frequencies near the carrier frequency is determined from the linearized equations [17]; we do this later in Sec. IV C. But first we turn to a discussion of the physics of Eq. (26), with particular emphasis on the differences between the usual NLSE and our Eqs. (26) and (27).

B. Discussion

In this section, we highlight the effects of the dispersion and nonlinearity in Eqs. (26) and (27), particularly those aspects not described by the usual NLSE. These include the consequences of the periodicity of the field ξ in time variable x; the effects of the dispersion parameters $\hat{\gamma}_1$ and $\hat{\gamma}_2$ describing the shape of the reflectivity spectrum, as well as the usual dispersion parameter—given here by the phase curvature $\hat{\phi}_2$; and the nature of the nonlinearity, which here is not instantaneous as in usual Kerr media, but arises due to carrier dynamics. In the spirit of previous work on nonlinear pulse propagation in optical fibers [17], we proceed by considering each physical effect separately.

In Eq. (26), ξ is the normalized, forward-propagating laser field at a particular location within the laser cavity ($z=0$) and the variation of ξ in x gives the field profile during one laser round trip time $0\leqslant x<1$ where $\xi(0,\tau)=\xi(1,\tau)$. The variation of ξ in time τ then gives the evolution of this field profile defined over $0\leqslant x<1$ in time τ. Since ξ is bounded in x with periodic boundary conditions, we may in general express ξ as a Fourier series

$$\xi(x,\tau)=\sum_\kappa \tilde{\xi}_\kappa(\tau)e^{-i\kappa x}, \qquad (28)$$

where the normalized frequency is given by $\kappa=2\pi m$ for integers m. Physically, the discrete values of κ identify the Fabry-Perot resonances of the laser cavity in the absence of any carrier dynamics or dispersion. As we illustrate below, these two effects are described by the τ time evolution of ξ, contained in the τ dependence of the coefficients of the individual frequency amplitudes $\tilde{\xi}_\kappa$. In Eq. (28), $\kappa=0$ labels the nominal lasing frequency—i.e., the frequency at which we assume the laser is initially oscillating, which is some cw frequency solution within the bandwidth of the reflection spectrum; we then assess the stability properties of this particular cw mode solution.

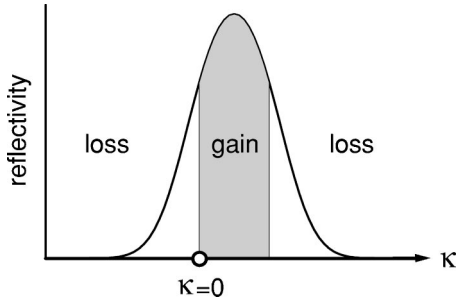

FIG. 9. Illustration of the effect on the laser field due to the reflection spectrum shape. For a nominal lasing frequency on the red side of the spectrum peak, indicated by the open circle, then the shaded region of the spectrum indicates the frequencies that experience gain (i.e., less loss than the nominal lasing frequency) when the field is reflected from the external cavity. The unshaded regions indicate which frequencies experience greater loss than the nominal lasing frequency. As a result of this selective loss, the carrier frequency of the field shifts toward the reflection spectrum peak.

First we present a discussion of the effects of dispersion of the external reflector by considering only the dispersive terms in Eq. (26), ignoring the nonlinearity. We rewrite Eq. (26) using the Fourier decomposition (28) to obtain [17]

$$\tilde{\xi}_\kappa(\tau)=\tilde{\xi}_\kappa(0)e^{(1/2)\kappa^2(-\hat{\gamma}_2+i\hat{\phi}_2)\tau}e^{-\hat{\gamma}_1\kappa\tau}. \qquad (29)$$

Recall that $\hat{\phi}_2$ appears in our equations as a result of the dispersion of the external cavity round trip time, so that upon evolution in τ, red and blue frequencies get separated in x time, that is, across the field profile, causing pulse chirping. The τ evolution of the pulse spectrum $|\tilde{\xi}_\kappa(\tau)|^2$, however, is only affected by $\hat{\gamma}_2$ and $\hat{\gamma}_1$, as is evident from Eq. (29). Recall that $\hat{\gamma}_2$ is the curvature of the (negative) logarithm of the reflection spectrum at the lasing mode, related to the spectral width, and $\hat{\gamma}_1$ is the slope, whose sign indicates the position of the nominal lasing frequency with respect to the peak of the reflection spectrum. As illustrated schematically in Fig. 9, mode frequencies with reflectivities larger than that of the chosen nominal lasing mode experience ''gain'' (i.e. less loss than the nominal lasing frequency), indicated by the shaded region, while those with smaller reflectivities experience greater loss. This selective loss tends to shift the lasing frequency to a mode closer to the reflection spectrum peak, if such a cavity mode exists. For a mode with frequency corresponding to the peak of the reflectivity spectrum, then $\hat{\gamma}_1=0$ and all frequencies except that mode experience loss; this causes a continual narrowing of the field spectrum as the side modes' amplitudes decay over time τ.

The fact that we have imposed periodic boundary conditions on the field in x also alters somewhat the usual description of the dispersive effects. Here, wavelengths with a shorter round trip time eventually get so far ahead in x of the wavelengths with a longer round trip time that they come full circle and catch up to the slower wavelengths again. In the absence of all physical effects except round trip time dispersion, the field profile then does not disperse indefinitely, but eventually the initial profile is recovered. This periodicity in τ can be seen analytically by considering the general expression for $\xi(x,\tau)$ in the time domain

$$\xi(x,\tau)=\sum_{m=-\infty}^{\infty}\tilde{\xi}_{2\pi m}(0)e^{-i2\pi mx}e^{i2\pi m^2(\pi\hat{\phi}_2\tau)},$$

where we replaced κ with $2\pi m$. Since m varies along the set of all integers, we see that as τ varies from 0 to $(\pi\hat{\phi}_2)^{-1}$, the exponent of the last term varies from 0 to an integer multiple of 2π, for all values of m. The smaller the $\hat{\phi}_2$ is, the longer it takes for the long and short wavelengths to separate from each other, and subsequently reunite.

We now describe the τ evolution of ξ in the special case for which we assume that the length of the external cavity is very long, so that the cw mode solutions within the bandwidth of the reflection spectrum are very dense, and these then approximate a continuous frequency variable. In this special limit, we consider (cf. Agrawal [17]) an initial field profile that is essentially uniform, but with a small, chirped perturbation centered at $x=1/2$,

$$\xi(x,0)=1+\xi_o\exp\left(-(1+iC)\frac{(x-1/2)^2}{2x_o^2}\right), \tag{30}$$

where x_o quantifies the initial width of the perturbation in x time domain and C is some real valued parameter characterizing the initial chirp. Solving Eq. (26) in frequency domain, keeping only the terms involving the dispersion parameters $\hat{\phi}_2$, $\hat{\gamma}_2$, and $\hat{\gamma}_1$, then using the (continuous) Fourier transform of Eq. (30) as the initial frequency spectrum, the evolved field at time $\tau>0$ has an x-time profile width that is dependent on the evolution time τ and is given by

$$x_o^2(\tau)=\frac{x_o^2+2(\hat{\gamma}_2+C\hat{\phi}_2)\tau+(\hat{\gamma}_2+\hat{\phi}_2)^2\tau^2(1+C^2)/x_o^2}{1+\hat{\gamma}_2\tau(1+C^2)/x_o^2}.$$

For $x_o^2(\tau)>x_o^2$, then the perturbation shape is broadened in the x domain, with a diminished peak amplitude, and thus the field eventually returns to the steady state. Conversely, for $x_o^2(\tau)<x_o^2$ the width of the perturbation in the x domain has decreased, and the peak amplitude increased, signifying a growth of the perturbation. Thus perturbation decay occurs for $\hat{\phi}_2>-\hat{\gamma}_2/C$, and (initial) perturbation growth occurs for $\hat{\phi}_2<-\hat{\gamma}_2/C$. Since the overall effect of $\hat{\gamma}_2$ is to narrow the spectrum and thereby broaden the time domain profile, the occurrence of either decay or growth of the perturbation depends not only upon the relative signs of $\hat{\phi}_2$ and the initial chirp C as for the usual NLSE, but also on their amplitudes. The effect of $\hat{\gamma}_1$ on the τ time evolved pulse is to shift the central frequency closer to the peak of the reflection spectrum, and it finally reaches the peak when $\tau\to\infty$, in the limit of a continuous κ variable. Note that this description of the narrowing or broadening in x domain of the perturbation width is valid only for a very dense cw mode distribution within the bandwidth of the reflection spectrum, corresponding to a very long laser cavity.

Finally, we turn to a discussion of the nonlinear term in Eq. (26) arising from the semiconductor response, considering for simplicity only the first order in the expansion of the exponential functions involving the carrier density σ. We then obtain for Eq. (26)

$$\frac{\partial\xi(x,\tau)}{\partial\tau}=\frac{1}{2}(1-i\beta_c)\sigma(x,\tau)\xi(x,\tau), \tag{31}$$

and neglecting terms of order $\sigma(|\xi|^2-1)$, Eq. (27) becomes

$$\frac{\partial\sigma(x,\tau)}{\partial x}=-\hat{\Gamma}_1\sigma(x,\tau)-\hat{\Gamma}_2[|\xi(x,\tau)|^2-1], \tag{32}$$

where $\hat{\Gamma}_1\equiv\Gamma_1\phi_1$ and $\hat{\Gamma}_2\equiv\Gamma_2\phi_1$ for the decay rates Γ_1, Γ_2 defined by Eq. (15). It is interesting to note that if we assume (incorrectly) that the carrier relaxation T_n is so rapid that the carriers are essentially always in steady state, i.e., the ''adiabatic'' limit, then Eqs. (31) and (32) give

$$\frac{\partial\xi(x,\tau)}{\partial\tau}=-\frac{1}{2}\frac{\hat{\Gamma}_2}{\hat{\Gamma}_1}(1-i\beta_c)[|\xi(x,\tau)|^2-1]\xi(x,\tau).$$

In this limiting case, the nonlinearity then resembles a Kerr-type nonlinearity.

Since we have seen in Sec. III that laser operation is always (linearly) stable for $\beta_c=0$, we determine the effects of semiconductor linewidth enhancement factor separately from the stimulated emission which provides gain or loss in ξ, depending upon the sign of σ. By considering only the $i\beta_c$ term in the $(1-i\beta_c)$ factor in Eq. (31), we can construct an analytic solution of Eq. (31) given formally by

$$\xi(x,\tau)=\xi(x,0)\exp\left[-i\frac{1}{2}\beta_c\int_0^\tau\sigma(x,\tau')d\tau'\right].$$

The linewidth enhancement factor β_c can thus be identified with a self-phase modulation effect, since $|\xi(x,\tau)|^2$ is unchanged by τ time evolution. The τ evolution does chirp the initial field profile, however, and creates an instantaneous frequency $\Delta\kappa$ that is given by

$$\Delta\kappa=-\frac{\partial}{\partial x}\arg[\xi(x,\tau)]=-\frac{\partial}{\partial x}\arg[\xi(x,0)]+\frac{1}{2}\beta_c\tau\frac{\partial\sigma(x,0)}{\partial x}, \tag{33}$$

where we have used $\sigma(x,0)$ in Eq. (33) since $\sigma(x,\tau)$ itself is constant in τ,

$$\sigma(x,\tau)=-\hat{\Gamma}_2\int_0^x e^{-\hat{\Gamma}_1(x-x')}[|\xi(x',0)|^2-1]dx'=\sigma(x,0),$$

due to the invariance of $|\xi|^2$. Then the initial field profile $\xi(x,0)$ influences the instantaneous frequency at all later τ times. While this seems to correspond to the usual self-phase modulation of an NLSE with a Kerr-type nonlinearity, the carrier dynamics themselves do play a role in laser stability determination in our system, as we illustrate in the following section.

C. Modulational instability

In the previous section, we present a linear stability analysis of the approximate Eqs. (26) and (27) and derive a stability condition that is analogous to, but not the same as, the modulational instability of uniform solutions of the usual NLSE. First, we confirm that the linear stability results based on Eqs. (26) and (27) agree on the whole with those of the exact model equations presented in Sec. III. Second, we examine the region of dispersion parameters over which we would expect stable laser cw operation.

Writing Eqs. (26) and (27) in terms of the field deviation from steady-state function, $\psi \equiv \xi - 1$, then linearizing in both σ and ψ, we obtain

$$\frac{\partial \psi(x,\tau)}{\partial \tau} = \frac{1}{2}(1 - i\beta_c)\sigma(x,\tau) - i\hat{\gamma}_1 \frac{\partial}{\partial x}\psi(x,\tau) + \frac{1}{2}(\hat{\gamma}_2 - i\hat{\phi}_2)\frac{\partial^2}{\partial x^2}\psi(x,\tau),$$

$$\frac{\partial \sigma(x,\tau)}{\partial x} = -\hat{\Gamma}_1 \sigma(x,\tau) - \hat{\Gamma}_2[\psi(x,\tau) + \psi^*(x,\tau)], \quad (34)$$

recall both σ and ψ vanish for steady state. To proceed, we assume that the field is of the form

$$\psi(x,\tau) = \varepsilon_1 e^{i\kappa x} e^{\zeta \tau} + \varepsilon_2 e^{-i\kappa x} e^{\zeta^* \tau}, \quad (35)$$

where the quantity ζ is some complex number that is to be determined as a function of κ. Again, the variable $\kappa = 2\pi m$ (for integers m) is discrete, corresponding to the Fabry-Perot resonances of the laser cavity, and the nominal lasing mode is denoted by $\kappa = 0$. The small numbers ε_1 and ε_2 give the amplitude of the excitations of ψ at modes κ and $-\kappa$ resulting from some small perturbation at $\tau = 0$. The response of the field to this side mode excitation is captured by the field's dependence on the longer time scale τ through the determined value of ζ [17]. For a given κ, $\mathrm{Re}\zeta(\kappa) > 0$ indicates that the mode at κ experiences exponential growth in the linear regime at a frequency corresponding to $-[\kappa + \mathrm{Im}\zeta(\kappa)]$, and thus the nominal lasing frequency is unstable to perturbations at this frequency. The $\mathrm{Im}\zeta$ provides a correction to the cavity resonance frequency, which arises due to effects of dispersion and carrier dynamics. A $\mathrm{Re}\zeta(\kappa) < 0$ then indicates that the amplitude of the mode at κ experiences exponential decay, and thus the laser is stable to excitations of the resonance at κ. Substituting Eq. (35) into Eq. (34), we obtain the quadratic equation

$$0 = \zeta^2 + \left(\frac{\hat{\Gamma}_2}{\hat{\Gamma}_1 + i\kappa} + \hat{\gamma}_2 \kappa^2\right)\zeta + \frac{1}{4}[(\hat{\phi}_2 - 2i\hat{\gamma}_1/\kappa)^2 + \hat{\gamma}_2^2]\kappa^2 \times \left[\kappa^2 + \frac{\hat{\gamma}_2 + \beta_c\hat{\phi}_2 - 2i\beta_c\hat{\gamma}_1/\kappa}{(\hat{\phi}_2 - 2i\hat{\gamma}_1/\kappa)^2 + \hat{\gamma}_2^2}\frac{2\hat{\Gamma}_2}{\hat{\Gamma}_1 + i\kappa}\right]. \quad (36)$$

Note that by substituting $i\omega$ for ζ, Eq. (36) can be rewritten in a form that corresponds more directly to the well-known modulational instability results of the problem of pulse propagation in optical fiber [17].

The discrete numerical solutions of Eq. (36) correspond directly with the singularities of Eq. (16) of the exact linear stability analysis, confirming the multiple scales analysis presented in Sec. IV A. The Laplace variable s from Sec. III is identified here with $(\zeta + i\kappa)/\phi_1$, so that $\phi_1 \mathrm{Re}s = \mathrm{Re}\zeta$ and $\phi_1 \mathrm{Im}s = \mathrm{Im}\zeta + \kappa$. The numerical solutions of both Eq. (36) and the singularities of Eq. (16), for parameters corresponding to the two lasers described in the caption of Fig. 8, are shown together in Figs. 10(a) and 10(b) for the negative and positive grating chirps, respectively. Figure 10 shows that the solutions of Eq. (36) give the same qualitative features as those described in Sec. III, although the two methods do not give exactly the same resonance locations. Nevertheless, the agreement is good enough to validate the discussion here and in the previous section. The discrepancy can be understood by noting that the more approximate solutions of Eq. (36) can be recovered from the exact linear stability analysis by expanding the denominator of Eq. (16) about a particular mode, and keeping only the first order in s. For example, Eq. (36) gives the decay rate of the nominal lasing mode to be $-\hat{\Gamma}_2/\hat{\Gamma}_1$, as does the first-order expansion of the $\mathrm{Im}s = 0$ pole of Eq. (16).

There are some special cases in which there seem to be extra solutions to Eq. (36) that do not correspond to poles of Eq. (16). In these special cases, the second set of poles (shadow resonances) and the zeros of $\hat{\psi}(s)$ in Eq. (16) are located at exactly the same position, both at solutions to $\tilde{r}^*(is^*) = \tilde{r}_o^*$, and so effectively cancel each other in the exact stability analysis. Recall that physically this occurs if we either ignore carrier-field coupling $\hat{\Gamma}_2$, or if the reflection spectrum is such that $\tilde{r}^*(is^*) = \tilde{r}(is)$, i.e., symmetric with no phase curvature. In these cases, the solutions of Eq. (36) gives both sets of poles, though in reality no shadow modes would be excited. We note that by choosing $\psi(x,\tau)$ to be of the form Eq. (35), only the growth or decay behavior of ψ can be determined, and this corresponds only to the singularities of $\hat{\psi}(s)$ of Eq. (16), but not the zeros. As long as we are not dealing with either of these special cases, however, the two methods give the same qualitative results.

In the remainder of this section, we expand our discussion of stability to include an examination of (i) the stability as a function of phase curvature, again for a cw mode coinciding with the reflection spectrum peak, and (ii) the stability of cw modes at arbitrary location within the reflection spectrum bandwidth, thus more fully assessing the stability of a particular laser. While the Laplace transform formalism of Sec. III may be used to investigate these issues, we choose to use

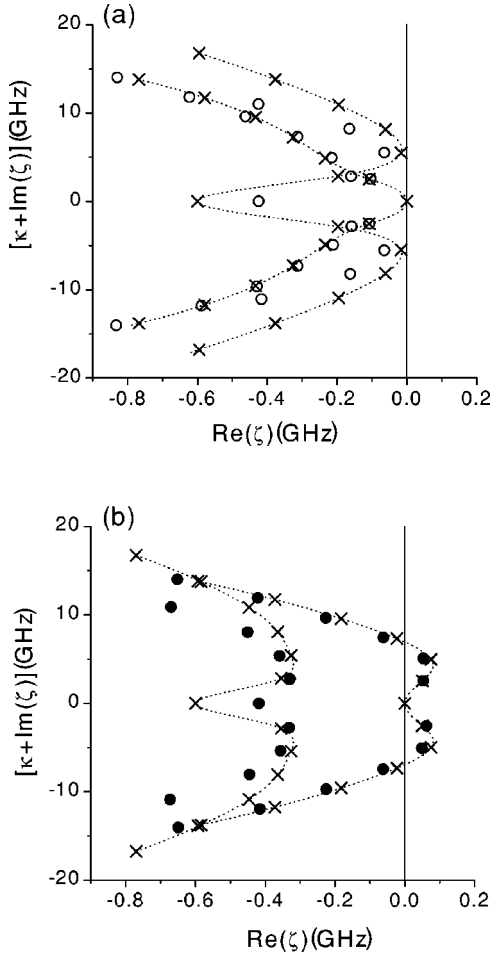

FIG. 10. (a) Comparison of the solutions for $\zeta(\kappa)$ for continuous (dotted lines) and discrete values (crosses) of κ, and the singularities of $\hat{\psi}(s)$ (open circles). The external cavity reflector corresponds to the reflection spectrum and phase of Fig. 3(a) with $\phi_2 = 770$ ps^2 and the laser diode parameters are as listed in Table I. (b) Solutions for $\zeta(\kappa)$ for continuous (dotted lines) and discrete (crosses) values of κ, and singularities of $\hat{\psi}(s)$ (filled circles) corresponding to Fig. 3(b) with $\phi_2 = -770$ ps^2. In both the cases, $\gamma_2 = 354$ ps^2.

instead the modulational instability results of this section. It is much less cumbersome to obtain numerical solutions of $\zeta(\kappa)$ using Eq. (36), than to calculate contours of $\hat{\psi}(s)$ and then find the singularities, even if the former method is slightly less accurate. From Eq. (36), we may also make a direct comparison with the well-known modulational instability of the usual NLSE.

We begin by seeking to understand how the width of the reflection spectrum, characterized by the dispersion parameter $\hat{\gamma}_2$, alters the modulational instability results of the usual NLSE, especially in light of the discussion of the previous section; recall that propagation of perturbed chirped pulses through the dispersive external cavity led to either the growth or decay of the perturbations, depending not only upon the relative signs of the chirp and dispersion parameter $\hat{\phi}_2$, but on their amplitudes with respect to $\hat{\gamma}_2$. To proceed, we consider the special case where the carrier dynamics is neglected (adiabatic limit) so that the nonlinearity is Kerr-like, and where the nominal lasing frequency coincides with the peak of the reflection spectrum so that $\hat{\gamma}_1 = 0$. Then the equation determining $\zeta(\kappa)$ becomes

$$0 = \zeta^2 + \left(\frac{\hat{\Gamma}_2}{\hat{\Gamma}_1} + \hat{\gamma}_2 \kappa^2 \right) \zeta + \frac{1}{4} (\hat{\phi}_2^2 + \hat{\gamma}_2^2) \times \kappa^2 \left[\kappa^2 + \frac{\hat{\gamma}_2 + \beta_c \hat{\phi}_2}{\hat{\phi}_2^2 + \hat{\gamma}_2^2} \frac{2\hat{\Gamma}_2}{\hat{\Gamma}_1} \right]. \tag{37}$$

Note that this is a quadratic equation of the form

$$f(x) = x^2 + bx + c,$$

where b and c are real valued coefficients, and $b > 0$ since the parameters $\hat{\gamma}_2$, $\hat{\Gamma}_1$, and $\hat{\Gamma}_2$ are all positive. Then for $b^2/4 - c < 0$ the roots of f are complex with a negative real part since b is positive, the roots are both real and negative for $0 < c \leq b^2/4$, and both roots are real, but one root is positive, for $c < 0$. From Eq. (37), we see then that this positive root can only occur when

$$\hat{\phi}_2 < -\hat{\gamma}_2 / \beta_c, \tag{38}$$

and for frequencies satisfying

$$|\kappa| < \sqrt{\frac{|\hat{\gamma}_2 + \beta_c \hat{\phi}_2|}{\hat{\phi}_2^2 + \hat{\gamma}_2^2} \frac{2\hat{\Gamma}_2}{\hat{\Gamma}_1}}. \tag{39}$$

This unstable region of $\hat{\phi}_2$ given by Eq. (38) is then analogous to the anomalous dispersion regime for negative dispersion parameter of the usual NLSE.

We now present a numerical example to examine the range of $\hat{\phi}_2$ over which a laser would be stable when the effects of carrier dynamics are included in the description. For the reflectivity spectrum (solid lines) shown in Figs. 3(a) and 3(b), and diode parameters listed in Table I, we calculate the parameters for a nominal lasing frequency at the peak of the reflection spectrum; then $\gamma_2 = 354$ ps^2, $\Gamma_1 = 14$ ns^{-1}, $\Gamma_2 = 22$ ns^{-1}, and $\beta_c = 2$. We then solve Eq. (36) for various values of $\hat{\phi}_2$, keeping these other parameters constant, and for each value of $\hat{\phi}_2$ determine whether or not there are any solutions of Eq. (36) such that $\mathrm{Re}(\zeta) > 0$, indicating instability. The range of $\kappa/2\pi$ over which $\mathrm{Re}(\zeta(\kappa)) > 0$ is indicated as a function of $\hat{\phi}_2$ by the shaded regions in Fig. 11. The dotted line in Fig. 11 is the unstable frequency region (39) for $\hat{\phi}_2$ within the range (38) that we would expect in the adiabatic limit. We find not only that there is instability for $\hat{\phi}_2 < -\hat{\gamma}_2 / \beta_c$, as expected, but that the stable range of $\hat{\phi}_2$ is also bounded from above; this upper bound has an absolute value much greater than $\hat{\gamma}_2 / \beta_c$, and must be the result of carrier dynamics, since it is not present in the adiabatic limit. The arrows in Fig. 11 indicate the values of the phase curvatures corresponding to the two laser configurations of Figs. 10(a) and 10(b); since the stable region for positive $\hat{\phi}_2$ is

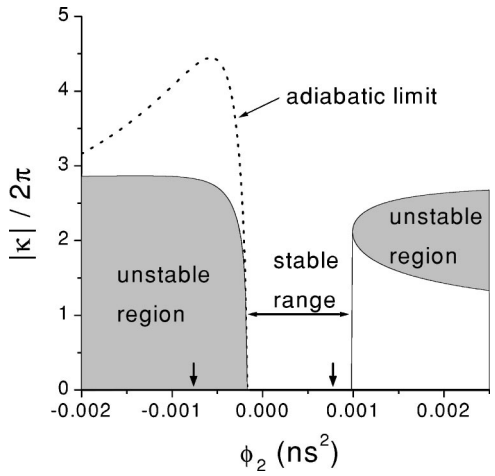

FIG. 11. The frequency domains in terms of $\hat{\phi}_2$ that are susceptible to modulational instability are as indicated by the shaded regions. Note that there is a bounded, stable range of $\hat{\phi}_2$ for which all excited resonances experience only decay. The dashed line gives the boundary of the (single) predicted unstable frequency domain in the adiabatic limit of no carrier dynamics. The arrows indicate the values of $\hat{\phi}_2$ for the gratings of Fig. 3(a) (right) and Fig. 3(b) (left).

much larger than the stable region for negative $\hat{\phi}_2$, then it is then apparent how orientation of the chirped fiber gratings would affect the laser stability.

We finally examine the stability of nominal lasing frequencies at arbitrary location within the range of the reflection spectrum. Recall that in our previous numerical examples, we have assessed the stability properties of a cw mode coinciding with the reflection spectrum peak. By extending the stability calculation for a particular laser to arbitrary frequency, we are more fully assessing the stability properties. We determine for which nominal lasing frequencies there would be unstable growth in any of the side modes: the range of frequencies for which there is only decay in the side modes indicates the region where we would expect cw laser operation might occur naturally. For each nominal lasing frequency, we must calculate the corresponding dispersion parameters $\hat{\gamma}_1$, $\hat{\gamma}_2$, $\hat{\phi}_2$ and decay rates $\hat{\Gamma}_1$, $\hat{\Gamma}_2$ and then use these parameters to find the discrete solutions $\zeta(\kappa)$ of Eq. (36). For each nominal lasing frequency, we find from the solutions $\zeta(\kappa)$ the greatest value of Re(ζ) over the domain κ, i.e., the greatest side mode exponential growth rate for a particular nominal lasing frequency; those frequencies that are unstable have $\max\{\mathrm{Re}\zeta(\kappa)\}>0$. We plot in Figs. 12(a) and 12(b) both $\max\{\mathrm{Re}\zeta(\kappa)\}$ and the reflectivity spectrum as a functions frequency, where $\max\{\mathrm{Re}\zeta(\kappa)\}=0$ if no growing solutions are found. We see from Fig. 12(a), not surprisingly, that for the laser with the negatively chirped grating where $\hat{\phi}_2>0$ (solid line), there exists a range of frequencies over which the laser would operate in stable cw operation, as indicated by the shaded region within the reflectivity spectrum in Fig. 12(b). For the positively chirped grating (dashed line), however, there is no such stable frequency range.

Notice, however, that the stable frequency range for the

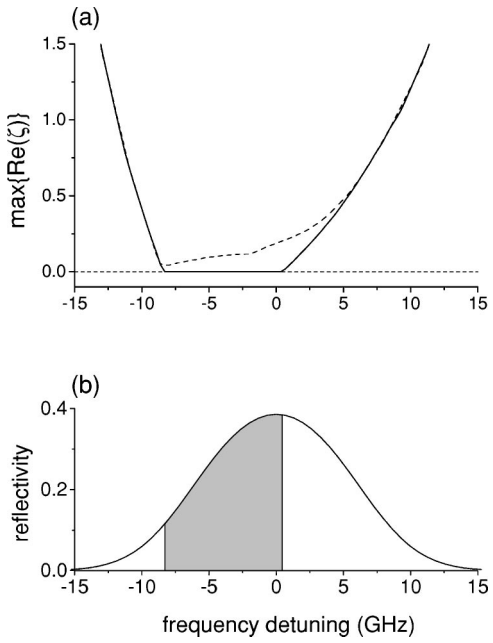

FIG. 12. (a) The maxima of Re(ζ) as a function of nominal lasing frequency, using the diode parameters listed in Table I, for both the negatively chirped grating of Fig. 3(a) (solid line) and the positively chirped grating of Fig. 3(b) (dashed line). Frequencies for which $\max(\mathrm{Re}(\zeta))>0$ are unstable to growth of side mode amplitudes. Note that only the negatively chirped grating has a stable frequency range; we see from (b), where we plot the corresponding reflectivity spectrum, that this stable range (shaded region) is located mainly on the red side of the reflectivity spectrum. The kinks result from a mode hop in the discrete side mode κ corresponding to the $\max(\mathrm{Re}(\zeta))$.

laser with $\hat{\phi}_2>0$ is located on mainly the *red* side of the reflection spectrum peak [24]. This can be understood by considering the time evolution of a pulse of light, with frequency off center from the reflection spectrum, as it propagates first through the external cavity, then subsequently through the diode. As discussed in the previous section, for a lasing frequency that is not at the reflection spectrum peak, the effect of the selective loss of the reflectivity spectrum is to pull the frequency toward the peak. Thus an initial frequency on the red side of the spectrum will be pulled toward the blue, and vice versa. In either case, though, the amount of loss experienced by the pulse decreases overall, causing a corresponding increase in the photon density. In turn, the increase in photon density causes an increased depletion of the carriers within the diode. Since the linewidth enhancement of the diode creates an instantaneous frequency shift that depends on the rate of change of the carriers according to Eq. (33), as we discussed earlier, there will be a red shifting that accompanies any decrease in the number of carriers. For an initial frequency on the red side of the reflection spectrum, then, these two effects tend to cancel each other out. For an initial frequency on the blue side, however, both the reflector and the diode are causing red shifts in the frequency, which over many round trip times would result in a hop of the lasing frequency to the red side of the reflectivity spectrum.

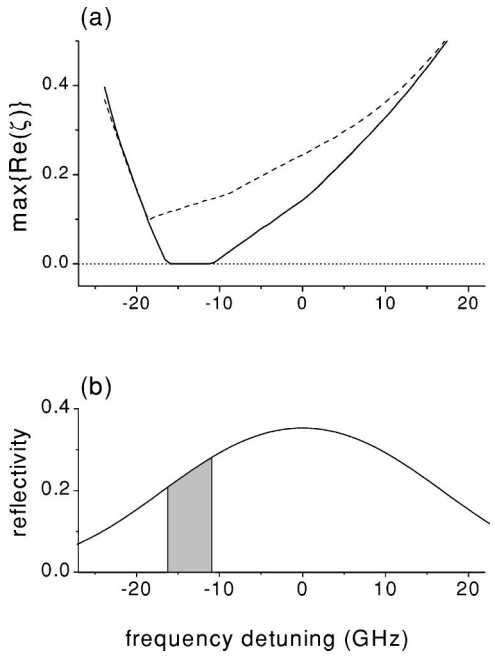

FIG. 13. (a) The maxima of Re(ζ) as a function of nominal lasing frequency, for a negatively (solid line) and positively (dashed line) chirped grating, each with a Bragg wavelength at the (Gaussian shaped) grating center of 1535 nm, a FWHM of 1 cm, a maximum index modulation depth of 4.8×10^{-5}, and a uniform background index of 1.44. The linear chirps are ±3.6 Å/cm, and diode parameters are as listed in Table I. These parameters correspond to the experimental configurations of Morton *et al.* [6], though we again neglect the dc background. Note that, again, only the negatively chirped grating has a stable frequency range. But from (b), where we plot the corresponding reflectivity spectrum, we find that this stable range (shaded region) is now located exclusively on the red side of the reflectivity spectrum.

To further emphasize the assymetry of the stable frequency range, we consider finally the stability of a different set of lasers, again with oppositely oriented fiber gratings, but now with fiber grating parameters corresponding directly to the experiments of Morton *et al.* [6]. The spectra of these two gratings have the same maximum reflectivity as in our previous example, but a larger absolute grating chirp leading to a larger spectral width. For this set of lasers, the calculation of ζ for the nominal lasing frequency at the reflection spectrum peak alone would indicate that *neither* orientation should result in stable cw operation. This does not give a full description of laser stability, however, since we need to consider the solutions of ζ for the full range of frequencies within the bandwidth of the reflector. We illustrate in Figs. 13(a) and 13(b) that although the negatively chirped grating cannot support stable cw operation at the reflection spectrum peak, it can support stable cw operation for a range of frequencies now *exclusively* on the red side of the reflection spectrum. Again, the laser with the positively chirped grating has no such stable frequency range. Thus, to explain the experimental results, it is necessary to consider this extended calculation of laser stability.

V. CONCLUSIONS

We have presented an original description of the stability properties of extended-cavity semiconductor lasers with dispersive loss, such as fiber grating semiconductor lasers. First, without assuming uniform gain within the semiconductor diode, we derived an expression for the Laplace transform of the electric-field response to small perturbations, written in terms of an arbitrary reflection function for the dispersive reflector. We used this formula to assess the stability of cw operation with respect to growth or decay of side modes, and deduced many laser properties from an examination of the growth or decay rates of these resonances. For example, we found that carrier-field coupling results in a more rapid decay of excited side modes closest to the nominal lasing frequency, while, not surprisingly, the incorporation of a finite reflection spectrum width causes modes farthest from the spectrum peak to decay most rapidly, since they experience the greatest loss. For reflection coefficients with nonzero phase curvature (corresponding to dispersion of the external cavity round trip time), the Fabry-Perot mode spacing itself is chirped, and secondary ''shadow resonances'' become excited due to the carrier-field interaction. This second set of resonances are also nonuniformly distributed along the frequency axis, but with a chirp opposite to that of the primary resonances. We have also shown that in the absence of linewidth enhancement in the semiconductor diode, the side modes always experience decay, indicating stability. In our final example, we found that for chirped fiber grating lasers, as in the experiments [6], the orientation of the grating chirp (and thus the sign of the reflection phase curvature) is a crucial parameter in the determination of laser stability, as expected.

In order to understand the role of the dispersion and linewidth enhancement factor in determining stability, we have included a more approximate model that turns out to be much more descriptive of the physical processes involved in instability. Based on our full laser equations, it is derived under the assumption that time scale of the onset of any instability is much longer than the round trip time of light in the extended laser cavity. We then derived an equation for the time evolution of the field that resembles a nonlinear Schrödinger equation. From this we found that the phase curvature of the reflection spectrum is analogous to the dispersion parameter of the NLSE, but unlike the usual modulational instability results of the NLSE, stability occurs only for a bounded range of this phase curvature. The lower bound of this range is determined by the reflection spectrum width and the linewidth enhancement factor, and is analogous to the boundary between anomalous and normal dispersion in the usual NLSE; the upper bound results from carrier dynamics, and is absent in the modulational instability results of NLSEs with instantaneous nonlinearities. The range is not symmetric about zero, but is centered on the positive side of the phase curvature scale. This is again in agreement with what experiments indicate. Finally, we found that for stable laser configurations, the laser oscillations tend to occur on the red side of the reflectivity spectrum. For parameters

corresponding to the experiments of Morton *et al*. [6], only the laser with a negatively chirped grating is stable, and laser oscillation in this case occurs exclusively on the red side of the reflection spectrum peak.

ACKNOWLEDGMENT

This work has been supported by the Natural Sciences and Engineering Research Council of Canada.

[1] F.N. Timofeev, I.S. Kostko, P. Bayvel, O. Berger, R. Wyatt, R. Kashyap, I.F. Lealman, and G.D. Maxwell, Electron. Lett. **35**, 1737 (1999).
[2] J.F. Lemieux, A. Bellemare, C. Latrasse, and M. Tetu, Electron. Lett. **35**, 904 (1999).
[3] H. Bissessur, C. Caraglia, B. Thedrz, J.M. Rainsant, and I. Riant, IEEE Photonics Technol. Lett. **11**, 1304 (1999).
[4] Z.F. Fan, P.J.S. Heim, J.H. Song, Y. Hu, F.G. Johnson, D.R. Stone, and M. Dagenais, IEEE Photonics Technol. Lett. **10**, 1784 (1998).
[5] R.J. Campell, J.R. Armitage, G. Sherlock, D.L. Williams, R. Payne, M. Robertson, and R. Wyatt, Electron. Lett. **32**, 119 (1996).
[6] P.A. Morton, V. Mizrahi, R. Tanbun-Ek, R.A. Logan, P.J. Lemaire, H.M. Presby, T. Erdogan, S.L. Woodward, J.E. Sipe, M.R. Phillips, A.M. Sergent, and K.W. Wecht, Appl. Phys. Lett. **64**, 2634 (1994).
[7] R. Kashyap, *Fiber Bragg Gratings* (Academic Press, San Diego, 1999).
[8] L. Ménager, L. Cabaret, I. Lorgeré, and J.-L. Le Gouët, Opt. Lett. **25**, 1246 (2000).
[9] P. Zorabedian, in *Tunable Lasers Handbook*, edited by F. J. Duarte (Academic Press, Toronto, 1995), pp. 349–442.
[10] P.S. Bhatia, G.R. Welch, and M.O. Scully, Opt. Commun. **189**, 321 (2001).
[11] D.M. Cornwell, Jr. and H.J. Thomas, Appl. Phys. Lett. **70**, 694 (1997).
[12] L. Ramunno and J.E. Sipe, IEEE J. Quantum Electron. **36**, 1299 (2000).
[13] A preliminary report of this work was presented in L. Ramunno and J.E. Sipe, Technical Report No. CLEO, 2001 (unpublished).
[14] L. Ramunno and J.E. Sipe, IEEE J. Quantum Electron. **35**, 624 (1999).
[15] K. Petermann, *Laser Diode Modulation and Noise* (Kluwer Academic, Boston, 1988).
[16] N. Dutta and G.P. Agrawal, *Semiconductor Lasers*, 2nd ed. (Van Nostrand Reinhold, New York, 1993).
[17] G.P. Agrawal, *Nonlinear Fiber Optics*, 3rd ed. (Academic Press, San Diego, 2001).
[18] R.W. Tkach and R.A. Chraplyvy, J. Lightwave Technol. **LT4**, 1655 (1986).
[19] G.H.M. van Tartwijk and D. Lenstra, Quantum Semiclassic. Opt. **7**, 87 (1995).
[20] L.M. Zhang and J.E. Carroll, IEEE J. Quantum Electron. **28**, 604 (1992).
[21] J.E. Sipe, L. Poladian, and C.M. de Sterke, J. Opt. Soc. Am. A **11**, 1307 (1994).
[22] The background index of refraction for the grating is uniform in this calculation—as is the case for current fiber grating fabrications—while it was nonuniform in the experiments [6]. We have found, however, that the inclusion of this dc background does not significantly alter the results we present.
[23] R.K. Dodd, J.C. Eibeck, J.D. Gibbon, and H.C. Morris, *Solitons and Nonlinear Wave Equations* (Academic Press, New York, 1982).
[24] It was shown that, for laser operation under large-scale modulation of the bias current, less adiabatic and dynamic chirp in the output field results if one considers the mode to be on the red side of the reflection spectrum [12,25].
[25] R.F. Kazarinov and C.H. Henry, IEEE J. Quantum Electron. **QE23**, 1401 (1987).